

# DISCOVERY OF RADIO/X-RAY/OPTICAL RESOLVED SUPERNOVA REMNANTS IN THE CENTER OF THE ANDROMEDA GALAXY

A.K.H. KONG

Harvard-Smithsonian Center for Astrophysics, 60 Garden Street, Cambridge, MA 02138; akong@cfa.harvard.edu

L.O. SJOUWERMAN

National Radio Astronomy Observatory, Socorro, NM 87801

B.F. WILLIAMS, M.R. GARCIA

Harvard-Smithsonian Center for Astrophysics, 60 Garden Street, Cambridge, MA 02138

AND

J.R. DICKEL

Department of Astronomy, University of Illinois at Urbana-Champaign, Urbana, IL 61801

*Draft version October 31, 2018*

## ABSTRACT

We have detected a spatially resolved supernova remnant (SNR) in the center of the Andromeda Galaxy, in radio, X-ray, and optical wavelengths. These observations provide the highest spatial resolution imaging of a radio/X-ray/optical SNR in that galaxy to date. The multi-wavelength morphology, radio spectral index, X-ray colors, and narrow-band optical imaging are consistent with a shell-type SNR. A second SNR is also seen resolved in both radio and X-ray. By comparing the morphological structure of the SNRs in different wavelengths and with that in our own Galaxy, we can study the shock morphologies of SNRs in the Andromeda Galaxy. The proximity of the SNRs to the core suggests high interstellar medium density in the vicinity of the SNRs in the center of the Andromeda Galaxy.

*Subject headings:* galaxies: individual (M31) — supernova remnants — X-rays: ISM

## 1. INTRODUCTION

Ground-based and spaced-based observations have allowed many supernova remnants (SNRs) in our Galaxy to be resolved, showing various different morphologies in radio, X-ray, and optical wavelengths (Weiler & Sramek 1988; van den Bergh 1988; Rho & Petre 1998). The expanding SNR shock can heat the surrounding interstellar medium (ISM) to temperatures up to  $10^8$  K and beyond, producing thermal X-ray emission, while synchrotron radiation seen in the radio band is due to the relativistic electrons accelerated behind the shock front in the magnetic field of the SNR. Optical emission from SNRs is from shocked-heated collisionally ionized species such as [S II], [N II] and [O III], as well as H $\alpha$  recombination emission. Multiwavelength observations of SNRs therefore provide important information on the structure of the ISM and chemical composition in the host galaxy, the evolutionary stage of the SNR, the character of the supernova ejecta and the nature of the progenitor and its associated stellar winds.

Most detailed studies of SNR have concentrated on our Galaxy simply because of the large angular size of the SNRs. However, studies of Galactic SNRs can be limited by the lack of reliable distance estimates, high interstellar absorption at optical and X-ray wavelengths, and the high level of confusion in many Galactic fields (Magnier et al. 1995). These limitations are overcome by studies of SNRs in nearby extragalactic systems such as the Large and Small Magellanic Clouds (e.g., Williams et al. 1999), and the Andromeda Galaxy (M31). At a distance of 780 kpc (Stanek & Garnavich 1998), M31 is the closest spiral galaxy that shares similar morphology, metallicity and size with the Milky Way; it is the best candidate for a comparative study of SNRs.

Studies of SNRs in M31 are mainly done in the optical (e.g., d’Odorico, Dopita, & Benvenuti 1980; Blair, Kirshner, & Chevalier 1981, 1982; Braun & Walterbos 1993; Magnier et al. 1995). About 200 SNR candidates have been identified by these surveys. In a recent extensive *ROSAT* Position Sensitive Proportional Counter (PSPC) survey (Supper et al. 2001) of M31, 16 X-ray SNRs were identified within a total area of  $\sim 10.7$  deg<sup>2</sup> by cross-correlating with these optical catalogs. Their X-ray luminosities (0.1–2.4 keV) range from  $10^{36}$  to  $10^{37}$  erg s<sup>-1</sup>. More recently, Kong et al. (2002a) discovered a spatially resolved X-ray SNR in M31 with *Chandra*. In the radio, Sjouwerman & Dickel (2001) found 3 SNRs near the center of M31. In this *Letter*, we report the discovery of the first radio/X-ray/optical resolved SNRs in the center of M31.

## 2. OBSERVATIONS AND RESULTS

### 2.1. Radio Data

At the distance of M31, the typical diameter of SNRs is between  $\sim 1$  arcsec and 20 arcsec so that some of the SNRs are large enough to be studied with high-resolution instruments in sufficient detail (Sjouwerman & Dickel 2001; Kong et al. 2002a). In particular, sensitive interferometric radio images have sufficient resolution to resolve the SNRs without suffering from the large scale diffuse background in the center of M31 (Hjellming & Smarr 1982; Crane, Dickel, & Cowan 1992; Crane et al. 1993). Very sensitive 8.4 GHz (3.6 cm) radio observations of the central 500 arcsec (1.9 kpc) of M31 were obtained by combining in total 120 hours of archival data taken with the Very Large Array (VLA) in its largest array configurations (A and B) between 1990 and 1996. The resulting radio image has an angular resolution of 0.24 arcsec and is sensitive

to angular sizes of up to 20 arcsec, and has an rms noise level of  $\sim 4 \mu\text{Jy/beam}$ . After discovering three faint radio SNRs in the 8.4 GHz archival data, we also observed the remnants for 24 hours with the VLA at 4.9 GHz (6 cm) in July 2002. The recent 4.9 GHz radio image (Fig. 1) is sensitive to angular structures from 1.2 to 36 arcsec and has an rms of  $\sim 5 \mu\text{Jy/beam}$ . Both radio images clearly show resolved shell-like objects that are brighter at 4.9 GHz than at 8.4 GHz (Sjouwerman & Dickel 2001). The largest SNR is located at 70 arcsec east-south-east of the nucleus of M31 at a position of R.A.=00<sup>h</sup>42<sup>m</sup>50<sup>s</sup>.41, Dec.=+41°15'56".4 (J2000), labeled object 1 in Fig. 1. The integrated flux density of the complex radio morphology is measured to be 1.13 mJy at 4.9 GHz. Its size of  $11.6 \times 8.4$  arcsec ( $44 \times 32$  pc) is consistent with a previous  $10.9 \times 7.8$  arcsec low-resolution (5 arcsec) VLA detection at 1.4 GHz designated Braun-101 (Braun 1990). With the notion that the flux density measured at 1.4 GHz might be confused with the extended background (Hjellming & Smarr 1982; Braun 1990), we derive a spectral index between 1.4 and 4.9 GHz of  $\alpha = -0.77$  or flatter, where  $S_\nu \propto \nu^\alpha$ . The radio morphology and radio spectral index are consistent with a shell-type SNR (Dickel & Milne 1998). It is worth noting that our radio observations also discover two more new SNRs, designated Braun-80 and Braun-95 (Braun 1990), near the nucleus of M31 (Sjouwerman & Dickel 2001).

## 2.2. X-ray Data

Following the discovery of the radio SNRs, we compare their radio positions with the M31 X-ray source positions as detected by the *Chandra* X-ray Observatory (Kong et al. 2002b; Kaaret 2002) and indeed the largest radio SNR, Braun-101, is spatially coincident with the X-ray source CXOM31 J004250.5+411556 (Kong et al. 2002b). We further examine a 40 ksec (37.7 ksec after rejecting high background period) *Chandra* X-ray image taken with the back-illuminated chip (S3) of the Advanced CCD Imaging Spectrometer (ACIS). The SNR is clearly detected in the 0.3–7 keV image and it is resolved as a ring-like object with a diameter of about 5 arcsec (Fig. 1). The SNR has about 55 background-subtracted photons (0.3–7 keV) in a  $3''$  radius extraction region. All of the emission from the SNR is confined to energies below  $\sim 1$  keV, indicating that it is a soft X-ray source (e.g., Di Stefano & Kong 2003). The shell-like X-ray morphology, soft X-ray nature, and good positional coincidence with the radio SNR makes the X-ray source as a secure X-ray counterpart of the radio identified SNR. We extracted the energy spectrum from a  $3''$  radius and background from an annulus centered on the source. In order to allow  $\chi^2$  statistics to be used, the spectrum was grouped into at least 10 counts per spectral bin. We fitted the data with a Raymond-Smith model and kept the  $N_H$  fixed at  $10^{21} \text{ cm}^{-2}$ . The best fit temperature is  $0.25^{+0.09}_{-0.06}$  keV (90% confidence) with a value of reduced chi-squared statistic  $\chi^2_\nu = 1.05$  for 5 degrees of freedom (d.o.f.). The 0.3–7 keV luminosity of the best fitting spectrum is  $(4.4^{+1.3}_{-2.2}) \times 10^{35} \text{ erg s}^{-1}$ . We also re-examined the 50 ksec *Chandra* High Resolution Camera (HRC) observation (Kaaret 2002) and Braun-101 is indeed visible as a faint extended source though it was not in the published HRC source list. Assuming the above spectral model, the corresponding 0.3–7 keV luminosity of the SNR is  $(7.1 \pm 2.5) \times 10^{35} \text{ erg s}^{-1}$ .

The other radio SNR, Braun-95, is also detected in the *Chandra* observation as an extended (with a diameter of  $\sim 10$  arcsec) object (marked as 2 in Fig. 1). Although it shows a clear

shell morphology in the radio image, the X-ray emission is very patchy. We extracted the energy spectrum with a  $4.5''$  radius circle centered on the source and background from a source-free region. We kept the  $N_H$  fixed at  $10^{21} \text{ cm}^{-2}$  and fitted the spectrum with Raymond-Smith model. The fit is rather poor ( $\chi^2_\nu = 1.55$  for 10 d.o.f.). We then added an additional power-law component and the fit was improved ( $\chi^2_\nu = 1.2$  for 8 d.o.f.). The best fit temperature is  $0.26^{+0.13}_{-0.07}$  keV, while the photon index is  $2.16^{+1.39}_{-2.16}$ ; the 0.3–7 keV luminosity is  $(8^{+7.0}_{-2.2}) \times 10^{35} \text{ erg s}^{-1}$ .

## 2.3. Optical Data

With the detection of radio and X-ray emissions from Braun-101, we searched the *Hubble Space Telescope* (HST) archive for any narrow-band exposures near that position. We found images taken with the Wide Field Planetary Camera 2 (WFPC2) in H $\alpha$  (F656N) filter. We downloaded the pipeline-calibrated images, registered them, and combined them with cosmic-ray rejection. The resulting continuum (F547M filter) subtracted image of the region around the SNR is shown in Figure 2. A resolved shell-like object with 3 arcsec diameter is seen at the radio and X-ray position in the H $\alpha$  image, indicating an optical counterpart of the SNR. The total H $\alpha$  flux is  $(7.3 \pm 0.5) \times 10^{-16} \text{ erg cm}^{-2} \text{ s}^{-1} \text{ \AA}^{-1}$ , while the peak H $\alpha$  surface brightness of the SNR is  $(3.3 \pm 0.4) \times 10^{-16} \text{ erg cm}^{-2} \text{ s}^{-1} \text{ arcsec}^{-2} \text{ \AA}^{-1}$  in the continuum-subtracted H $\alpha$  image. Re-examination of ground-based narrow-band optical images from the Kitt Peak National Observatory 0.6-m Burrell Schmidt telescope also reveals Braun-101 (but unresolved) with [S II]/H $\alpha \sim 0.65$ . This high ratio makes it unlikely that the H $\alpha$  emission is from a HII region near the SNR (Levenson et al. 1995), and confirms the radio/X-ray identification as a SNR. Unfortunately, radio/X-ray SNR, Braun-95, is just outside the field of view of the *HST* observations.

## 3. DISCUSSION

Using VLA, *Chandra*, and *HST* data, we found one radio/X-ray/optical resolved SNR (Braun-101) and one radio/X-ray resolved SNR (Braun-95) near the center of M31. The radio emission of Braun-101 traces the outer shell of the remnant; it is an asymmetric shell with the northeastern side about three times brighter ( $67$  versus  $23 \mu\text{Jy/beam}$ ) than the southwestern side. The X-ray remnant with a diameter of about 5 arcsec (20 pc) is considerably smaller than the radio remnant and the X-ray outline lies predominantly inside the brighter part of the radio remnant. Both wavelengths show a shell configuration but the X-ray remnant is elongated toward the north, while the southern part of the X-ray remnant near the center of the radio remnant is slightly brighter in X-ray. It could be that the situation is similar to that seen for SNR 1E0102.2-7219 in the Small Magellanic Cloud (Amy & Ball 1999; Gaetz et al. 2000). The X-ray emission is brightest in a ring primarily inside the radio shell but very faint X-rays are seen extending out to the shock just outside the radio shell. The bright inner X-ray ring is interpreted as coming from heating and ionization from the reverse shock moving into a strong gradient in pre-explosion ejecta of the progenitor star. A longer X-ray exposure might reveal the expected faint outer X-ray emission. The larger radio shell is perhaps the forefront of the shock in a relatively low ISM density toward southwest, where the greatest magnetic field compression and particle acceleration occurs.

The optical emission of Braun-101 is the smallest (3 arcsec; 11 pc) compared to other wavelengths and it is encompassed

by the X-ray emission (Fig. 2). The  $H\alpha$  shell roughly traces the inner X-ray ring of the remnant and shows a non-uniform distribution of emission over the shell, with slight enhancement toward the southwest. It also shows a crescent opening and possibly a double-ring structure in the northern region of the optical remnant. In the northeast, a local enhancement of the X-ray emission corresponds to a local optical enhancement. The optical emission could be produced by shocks driven into cooler and denser material by the high pressure downstream of the reverse shock. It is worth noting that such large discrepancies in SNR size at different wavelengths are not typical (Winkler & Long 1997). In this case, we may be seeing only the brightest optical knots and not the whole optical shell.

Braun-101 is only 0.5 arcsec from an optically identified planetary nebula candidate (Kong et al. 2002b; Ciardullo et al. 1989). Our multiwavelength observations provide strong evidence that the source is actually a SNR. As planetary nebulae are usually identified by their strong [O III] emission (Ciardullo et al. 1989), they could resemble the [O III] emission from some SNRs. However, the large angular size (from 10 pc in the optical to 40 pc in the radio) and high X-ray luminosity ( $4.4 \times 10^{35}$  erg s $^{-1}$ ) rule out the possibility of a planetary nebula for which the typical diameter and X-ray luminosity is  $< 1$  pc ( $< 0.25$  arcsec) and  $10^{30}$  erg s $^{-1}$ , respectively.

Like Braun-101, Braun-95 is clearly a shell-like radio remnant (see Fig. 1) and its morphology is also very similar to Braun-101. The X-ray remnant of Braun-95, however, is patchy and is mainly located in the northeastern side of the radio remnant, where the radio emission is brightest. Faint X-ray emission is also seen near the radio shell. The X-ray spectrum likely consists of two components: a Raymond-Smith model and a power-law model. The Raymond-Smith temperature is similar to Braun-101 and CXOM31 J004327.7+411829 (Kong et al. 2002a). The extra power-law component might hint that Braun-95 contains a pulsar and/or a pulsar nebula.

Discovery of SNRs near the center of M31 provides some information about the star formation history of the region. For instance, type Ia SNRs suggest an old stellar population, while type Ib/II SNRs are associated with young population. Unfortunately, we do not have direct evidence about the type for the

two SNRs based on the current multi-wavelength data. By comparing with Galactic SNRs, the mismatch in morphology of the two SNRs in different wavelengths might hint the type. For example, IC 443 (Petre et al. 1988; Kawasaki et al. 2002) and Sgr A East (Maeda et al. 2002) are type II SNRs that have different morphology in radio and X-ray, and type Ia SNR like Tycho and SN 1006 generally have a well matched morphology in X-ray and radio. On the other hand, the X-ray and radio surface brightness of Tycho does not show correspondence (Hwang & Gotthelf 1997), and the X-ray emission of SN 1006 is non-thermal (Long et al. 2003), suggesting a synchrotron origin of X-rays. In addition, type Ib/II SNRs such as Cas A (compare Hughes, et al. 2000 and Braun, Gull & Perley 1987; see also Keohane et al. 1996 and Dickel et al. 1982) and RCW103 (compare Dickel et al. 1996 and Tuohy & Garmire 1980) also have a good match in different wavelengths. Further multi-wavelength observations of these 2 SNRs are required to identify their type and hence the associated stellar population in the bulge of M31.

The multiwavelength detection of SNRs in M31 can also provide further information about the local ISM density around the SNRs. The ISM near M31's SNRs is thought to be low ( $< 0.1$  cm $^{-3}$ ), which is 1 to 2 orders of magnitude smaller than the measurements by the HI observations (Magnier et al. 1997). Our discovery of X-ray emission from SNRs near the nucleus of M31 indicates that the ISM density in the vicinity of the SNRs could be higher.

We have shown that by combining all the high-resolution instruments across many wavebands, we can study the morphological structure of SNRs in M31 for the first time. This is a first step toward understanding the evolutionary states and shock morphologies of SNRs in M31. More specific multiwavelength observations in the future will shed more light on the properties of SNRs in M31, allowing more comprehensive comparative studies with our own Galaxy.

This research was supported by NASA under LTSA grants, NAG5-10889 and NAG5-10705. A.K.H.K. acknowledges support from the Croucher Foundation.

## REFERENCES

- Amy, S., & Ball, L., 1999, *ApJ*, 411, 761  
 Blair, W.P., Kirshner, R.P., & Chevalier, R.A. 1981, *ApJ*, 247, 879  
 Blair, W.P., Kirshner, R.P., & Chevalier, R.A. 1982, *ApJ*, 254, 50  
 Braun, R., & Walterbos, R.A.M. 1993, *A&AS*, 98, 327  
 Braun, R. 1990, *ApJS*, 72, 761  
 Braun, R., Gull, S.F., Perley, R.A. 1987, *Nature*, 327, 395  
 Ciardullo, R., Jacoby, G.H., Ford, H.C., & Neill, J.D., 1989, *ApJ*, 339, 53  
 Crane, P.C., Dickel J.R., & Cowan, J.J., 1992, *ApJ*, 390, L9  
 Crane, P.C., Cowan, J.J., Dickel, J.R., & Roberts, D.A., 1993, *ApJ*, 417, L61  
 Dickel, J.R., & and Milne, D.K., 1998, *AJ*, 115, 1057  
 Dickel, J.R., Green, A., Ye, T., Milne, D.K. 1996, *AJ*, 111, 340  
 Dickel, J.R., Murray, S.S., Morris, J., Wells, D.C. 1982, *ApJ*, 257, 145  
 Di Stefano, R., & Kong, A.K.H., 2003, *ApJ*, in press (astro-ph/0301162)  
 d'Odorico, S., Dopita, M.A., & Benvenuti, P. 1980, *A&AS*, 40, 67  
 Gaetz, T.J., Butt, Y.M., Edgar, R.J., Eriksen, K.A., Plucinsky, P.P., Schlegel, E.M., & Smith, R.K., 2000, *ApJ*, 543, L47  
 Hjellming, R.M., & Smarr, L.L., 1982, *ApJ*, 257, L13  
 Hughes, J.P., Rakowski, C.E., Burrows, D.N., & Slane, P.O. 2000, *ApJ*, 528, L109  
 Hwang, U., & Gotthelf, E.V. 1997, *ApJ*, 475, 665  
 Kaaret, P., 2002, *ApJ*, 578, 114  
 Kawasaki, T.K., Ozaki, M., Nagase, F., Masai, K., Ishida, M., & Petre, R. 2002, *ApJ*, 572, 897  
 Keohane, J.W., Rudnick, L., & Anderson, M.C. 1996, *ApJ*, 466, 309  
 Kong, A.K.H., Garcia, M.R., Primini, F.A., & Murray, S.S., 2002a, *ApJ*, 580, L125  
 Kong, A.K.H., Garcia, M.R., Primini, F.A., Murray, S.S., Di Stefano, R., & McClintock, J.E., 2002b, *ApJ*, 577, 738  
 Lauer, T.R., et al., 1993, *AJ*, 106, 1436  
 Levenson, N.A., Krishner, R.P., Blair, W.P., & Winkler, P.F., 1995, *AJ*, 110, 739  
 Long, K.S., Reynolds, S.P., Raymond, J.C., Winkler, P.F., Dyer, K.K., & Petre, R. 2003, *ApJ*, 586, 1162  
 Maeda, Y., et al. 2002, *ApJ*, 570, 671  
 Magnier, E.A., Prins, S., van Paradijs, J., Lewin, W.H.G., Supper, R., Hasinger, G., Pietsch, W., & Truemper, J., 1995, *A&AS*, 114, 215  
 Magnier, E.A., Primini, F.A., Prins, S., van Paradijs, J., & Lewin, W.H.G., 1997, *ApJ*, 490, 649  
 Petre, R., Szymkowiak, A.E., Seward, F.D., & Willingale, R. 1988, *ApJ*, 335, 215  
 Rho, J., & Petre, R., 1998, *ApJ*, 503, L167  
 Stanek, K.Z., & Garnavich, P.M., 1998, *ApJ*, 503, L131  
 Supper, R., Hasinger, G., Lewin, W.H.G., Magnier, E.A., van Paradijs, J., Pietsch, W., Read, A.M., & Trumper, J. 2001, *A&A*, 373, 63  
 Sjouwerman, L.O., & Dickel, J.R., 2001, in *Young Supernova Remnants*, eds. S.S. Holt and U. Hwang, AIP Conference Proceedings, Vol. 565, p.433  
 Tuohy, I., & Garmire, G. 1980, *ApJ*, 239, L107  
 van den Bergh, S., 1988, *ApJ*, 327, 156  
 Weiler, K.W., & Sramek, R.A., 1988, *ARA&A*, 26, 295  
 Williams, R.M., Chu, Y., Dickel, J.R., Petre, R., Smith, R.C., & Tavarez, M., 1999, *ApJS*, 123, 467  
 Winkler, P.F., & Long, K.S., 1997, *ApJ*, 491, 829

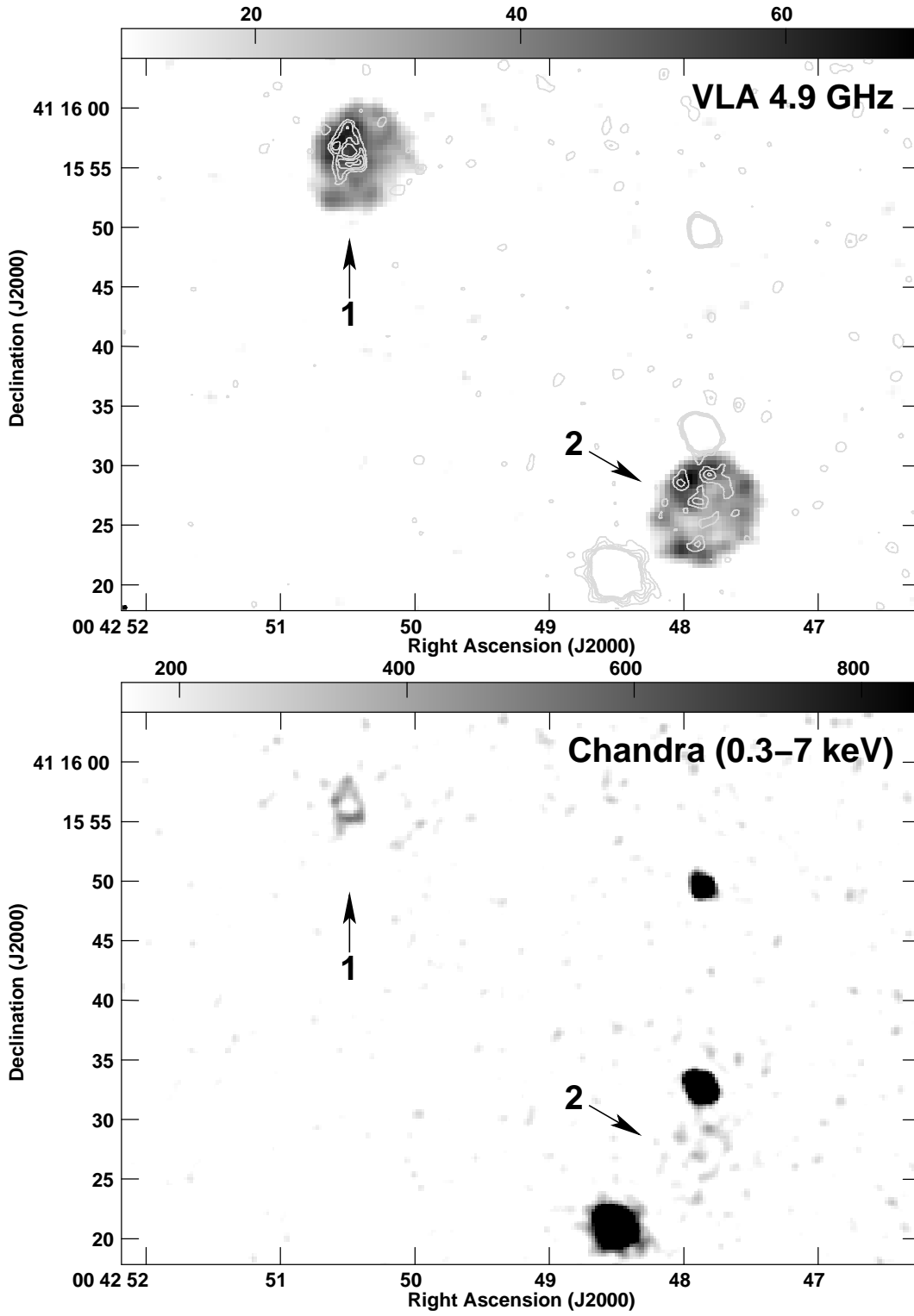


FIG. 1.— Top: VLA 4.9 GHz (1.2 arcsec resolution) radio image (grey scale from 10 to 70 microJy) of CXOM31 J004250.5+411556 (marked as 1) and nearby region with the *Chandra* X-ray contours. The contour map was created from a smoothed image with a 0.5 arcsec  $\sigma$  Gaussian function. Contours are at 0.6, 0.9, 1.2, and  $1.5 \times 10^{-5}$  counts  $\text{sec}^{-1} \text{arcmin}^{-2}$ . Also shown in the figure is another radio SNR, Braun-95 (Sjouwerman & Dickel 2001; Braun 1990), on the southwestern side (marked as 2). The radio position of the SNR is R.A.=00<sup>h</sup>42<sup>m</sup>47<sup>s</sup>.82, Dec.=+41° 15′ 25″.7 (J2000). To match the radio and X-ray images, we used the nucleus of M31 (M31\*) to cross-register both images. The two arrows have a length of 5″. Bottom: *Chandra* 0.3- to 7-keV image of the same field as the above radio image. The image has been smoothed with a 0.5 arcsec  $\sigma$  Gaussian function. The scales of both images are the same.

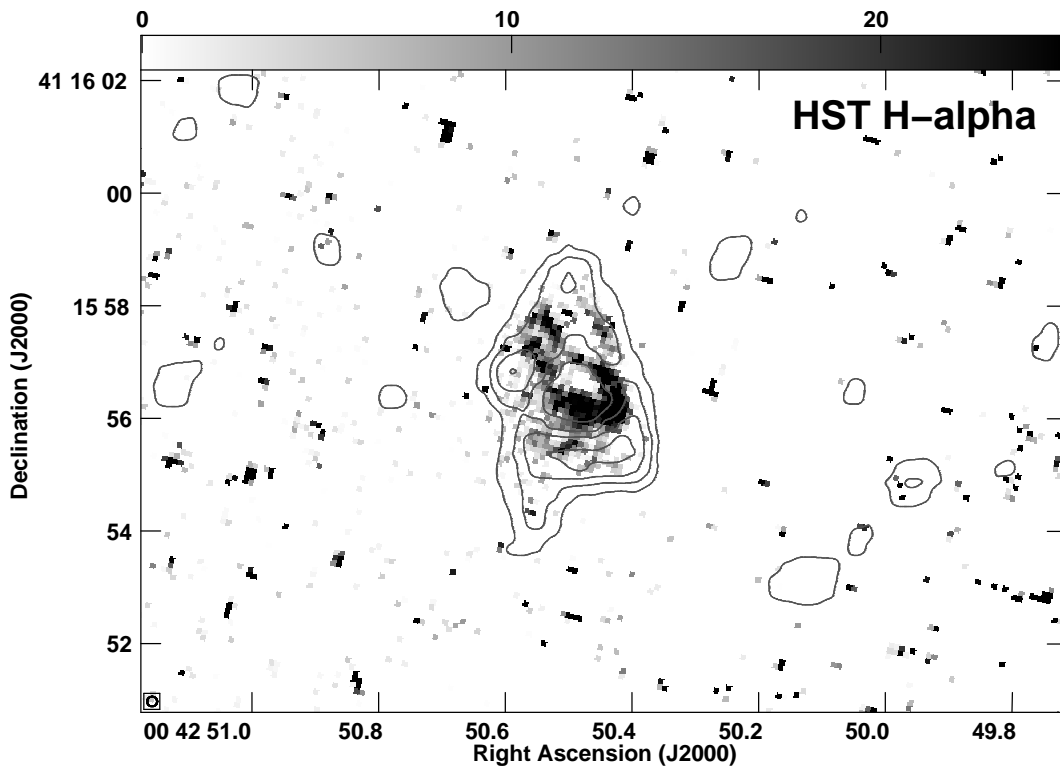


FIG. 2.— *HST* continuum-subtracted  $H\alpha$  image of the blow up region of CXOM31 J004250.5+411556 with the *Chandra* X-ray contours (same as Fig. 1). We used the X-ray position of M31\* (Kong et al. 2002) and optical position of the double nucleus P2 (Lauer et al. 1993) to match both images.